Conceptual design and simulation of a water Cherenkov muon veto for the XENON1T experiment

E. Aprile[a], F. Agostini[b]*, M. Alfonsi[c], K. Arisaka[d], F. Arneodo[e†], M. Auger[f], C. Balan[g],
P. Barrow[f], L. Baudis[f], B. Bauermeister[h], A. Behrens[f], P. Beltrame[i‡], K. Bokeloh[l],
A. Breskin[i], A. Brown[m], E. Brown[l], S. Bruenner[n], G. Bruno[e], R. Budnik[i],
J. M. R. Cardoso[g], A.P. Colijn[c], H. Contreras[a], J.P. Cussonneau[o], M.P. Decowski[c],
E. Duchovni[i], S. Fattori[h§], A. D. Ferella[e], W. Fulgione[p], M. Garbini[b], C. Geis[h],
L. W. Goetzke[a], C. Grignon[h], E. Gross[i], W. Hampel[n], R. Itay[i], F. Kaether[n],
G. Kessler[f], A. Kish[f], H. Landsman[i], R. F. Lang[m], M. Le Calloch[o], D. Lellouch[i],
L. Levinson[i], C. Levy[l], S. Lindemann[n], M. Lindner[n], J. A. M. Lopes[g¶], K. Lung[d],
A. Lyashenko[d], S. MacMullin[m], T. Marrodán Undagoitia[n], J. Masbou[o], F. V. Massoli[b],
D. Mayani Paras[f], A. J. Melgarejo Fernandez[a], Y. Meng[d], M. Messina[a], B. Miguez[p],
A. Molinario[p], G. Morana[b], M. Murra[l], J. Naganoma[q], U. Oberlack[h], S. E. A. Orrigo[g∥]
E. Pantic[d], R. Persiani[b], F. Piastra[f], J. Pienaar[m], G. Plante[a], N. Priel[i], S. Reichard[m],
C. Reuter[m], A. Rizzo[a], S. Rosendahl[l], J. M. F. dos Santos[g], G. Sartorelli[b],
S. Schindler[h], J. Schreiner[n], M. Schumann[r], L. Scotto Lavina[o], M. Selvi[b], P. Shagin[q],
H. Simgen[n], A. Teymourian[d], D. Thers[o], A. Tiseni[c], G. Trinchero[p], O. Vitells[i],
H. Wang[d], M. Weber[n], C. Weinheimer[l].

(The XENON1T Collaboration)
[a]*Physics Department, Columbia University, New York, NY, USA,*
[b]*Department of Physics, University of Bologna and INFN-Bologna, Bologna, Italy,*
[c]*Nikhef and the University of Amsterdam, Science Park, Amsterdam, Netherlands,*
[d]*Physics & Astronomy Department, University of California, Los Angeles, CA, USA,*
[e]*INFN – Laboratori Nazionali del Gran Sasso, 67010 Assergi, Italy,*
[f]*Physik-Institut, University of Zurich, Zurich, Switzerland,*
[g]*Department of Physics, University of Coimbra, Coimbra, Portugal,*
[h]*Institut für Physik & Exzellenzcluster PRISMA, Johannes Gutenberg-Universität Mainz, Mainz,
 Germany,*
[i]*Department of Particle Physics and Astrophysics, Weizmann Institute of Science, Rehovot, Israel,*
[l]*Institut für Kernphysik, Wilhelms-Universität Münster, Münster, Germany,*
[m]*Department of Physics and Astronomy, Purdue University, West Lafayette, IN, USA,*
[n]*Max-Planck-Institut für Kernphysik, Heidelberg, Germany,*
[o]*SUBATECH, Ecole des Mines de Nantes, CNRS/In2p3, Université de Nantes, Nantes, France,*
[p]*INFN-Torino and Osservatorio Astrofisico di Torino, Torino, Italy,*
[q]*Department of Physics and Astronomy, Rice University, Houston, TX, USA,*
[r]*Albert Einstein Center for Fundamental Physics, University of Bern, Bern, Switzerland.*
 E-mail: `fattori@uni-mainz.de, dr.serena.fattori@gmail.com`

ABSTRACT: XENON is a direct detection dark matter project, consisting of a time projection chamber (TPC) that uses xenon in double phase as a sensitive detection medium. XENON100, located at the Laboratori Nazionali del Gran Sasso (LNGS) in Italy, is one of the most sensitive experiments of its field, with published limits of $2 \cdot 10^{-45}$ cm^2 for the spin-independent WIMP-nucleon cross section for a WIMP mass of 55 GeV/c^2 and $3.5 \cdot 10^{-40}$ cm^2 for the spin-dependent WIMP-neutron cross section for a WIMP mass of 45 GeV/c^2. During the operation of XENON100, the design and construction of the next generation detector (of ton-scale mass) of the XENON project, XENON1T, is taking place. XENON1T is being installed at LNGS as well. It has the goal to reduce the background by two orders of magnitude compared to XENON100, aiming at a sensitivity of $2 \cdot 10^{-47}$ cm^2 for a WIMP mass of 50 GeV/c^2. With this goal, an active system that is able to tag muons and their induced backgrounds is crucial. This active system will consist of a water Cherenkov detector realized with a water volume $\sim$10 m high and $\sim$10 m in diameter, equipped with photomultipliers of 8 inches diameter and a reflective foil. In this paper we present the design and optimization study for this muon veto water Cherenkov detector, which has been carried out with a series of Monte Carlo simulations, based on the GEANT4 toolkit. This study showed the possibility to reach very high detection efficiencies in tagging the passage of both the muon and the shower of secondary particles coming from the interaction of the muon in the rock: $> 99.5\%$ for the former type of events (which represent $\sim 1/3$ of all the cases) and $> 70\%$ for the latter type of events (which represent $\sim 2/3$ of all the cases). In view of the upgrade of XENON1T, that will aim to an improvement in sensitivity of one order of magnitude with a rather easy doubling of the xenon mass, the results of this study have been verified in the upgraded geometry, obtaining the same conclusions.

KEYWORDS: Cherenkov and transition radiation, Detector modelling and simulations, Cherenkov detectors, Dark Matter detectors.

*Present address: Gran Sasso Science Institute, L'Aquila, Italy

†Present address: New York University in Abu Dhabi, UAE

‡Present address: School of Physics & Astronomy, The University of Edinburgh, Edinburgh, United Kingdom

§Corresponding author.

¶also with Coimbra Engineering Institute, 3030-199 Coimbra, Portugal

‖Present address: IFIC, CSIC-Universidad de Valencia, Valencia, Spain

Contents

1. Introduction

The XENON project is devoted to the direct detection of Weakly Interactive Massive Particles (WIMPs), a prime cold dark matter candidate arising, e.g., from theories of supersymmetry (SUSY) or Universal Extra Dimensions (UED) [1].

Recently the results from noble liquid detectors have shown the promising performances of this technology. Among these we recall the first experiment of the XENON project, based on the prototype detector XENON10 operated at LNGS [2], [3]. The subsequent detector, XENON100 (of 100 kg scale mass), is currently taking dark matter data at LNGS. XENON100 has completed a dark matter run with 225 live days of data that led to the publication of the world's best limit, in 2012, for spin-independent elastic WIMP-nucleon scattering cross section of $2.0 \cdot 10^{-45}$ cm^2 for a WIMP mass of 55 GeV/c^2 at 90% confidence level [4] and, in 2013, for the spin-dependent WIMP-neutron scattering cross section of $3.5 \cdot 10^{-40}$ cm^2 for a WIMP mass of 45 GeV/c^2 at 90% confidence level [5].

During the operation of XENON100, the design and construction of XENON1T is taking place. This new generation detector aims to reach the sensitivity of $2 \cdot 10^{-47}$ cm^2 for a WIMP mass of 50 GeV/c^2 at 90% confidence level [6]. To achieve this goal, a background reduction of two orders of magnitude compared to XENON100 [7], [8] is required.

The design of the detector and the selection of radiopure materials are crucial issues to accomplish this request. Another important aspect is the shielding against cosmic rays and natural radioactivity. The XENON1T detector is being placed underground in Hall B of LNGS. The residual flux of muons that reach the experimental hall is $(3.31 \pm 0.03) \cdot 10^{-8} \ \mu/(cm^2 \ s)$ (according to [9], [10] and [11]) with an average energy of $\sim$270 GeV [12]. Moreover, the detector will be installed in the center of a large cylindrical tank filled up with water. Figure 1 is the result of a dedicated simulation showing the absorption of neutrons and γ from rock radioactivity and of muon-induced neutrons as a function of the water shield thickness. It is apparent that few meters of water constitute an effective shield against gamma and neutrons produced by rock radioactivity. The only residual background after 5 meters of water is given by muon-induced neutrons, which are produced via direct muon spallation of nuclei or through electromagnetic and hadronic cascades generated by muons. A conservative estimation of the muon-induced neutron flux is $\sim 7.3 \cdot 10^{-10}$ n/(cm^2 s) for $E_n > 10$ MeV [14], that is about 3 orders of magnitude lower than that of neutrons from concrete radioactivity, but their energy spectrum extends up to tens of GeV. They constitute a dangerous background since they can scatter elastically off the target nuclei leaving a WIMP-like signal. This fact motivated to operate the water tank as an active muon-veto by detecting the Cherenkov light that charged particles produce as they cross the water. The aim is to be able to identify events in which a muon directly crosses the water tank, and also events in which a muon is outside but the particles constituting the electromagnetic or hadronic cascade enter the water tank.

In this work we present the study performed to design the muon-veto for the XENON1T experiment. A detailed Monte Carlo simulation has been set up in order to optimize the working configuration. In particular, the total number and the arrangement of photomultipliers (PMTs) and the possibility to use a reflective foil have been discussed. Following the outcomes of the simulation, different possible trigger conditions have been evaluated. The study has been extended to the case of a future upgrade of XENON1T, the XENONnT experiment, that will aim to an improvement in sensitivity of one order of magnitude with a rather easy doubling of the xenon mass.
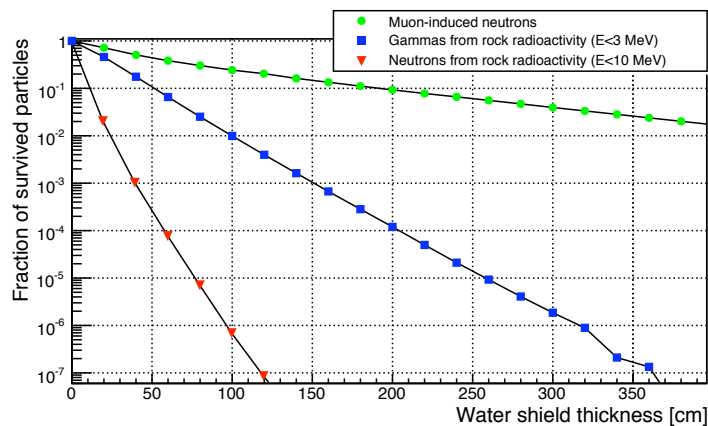

Figure 1: Fraction of survived particles as a function of the thickness of the water shield surrounding the detector. Circular dots for the muon-induced neutrons, squared dots for the gammas from rock radioactivity and triangular dots for neutrons from rock radioactivity.

2. Muon veto conceptual design

In the XENON1T experiment, the liquid xenon detector will be placed at the center of a large cylindrical tank with a radius of 4.8 m and about 9 m height plus a truncated cone shape on the top for a total height of 10.5 m, filled with water up to 10.2 m (see figure 2). In such a way, the XENON1T detector will be surrounded on all sides with a layer of pure water, which will constitute a shielding system against external radioactivity. Moreover, by equipping the water tank with an array of PMTs, the water could be exploited as a Cherenkov medium to detect the optical photons produced by cosmic muons and their secondary showers during their passage through water.

The selected photomultiplier is the high quantum efficiency (HQE) 8" Hamamatsu R5912ASSY, already provided with a water-proof enclosure. These PMTs have a bialkali photocathode and borosilicate glass window. Ten dynodes provide a typical gain of 10^7 at a working voltage of $\sim$1500 V. The quantum efficiency is about 30%, averaged over the Cherenkov light wavelength distribution, in the range [300-600] nm (see figure 3), and the collection efficiency is 85%, as declared by the manufacturer [15]. With respect to the trigger condition for the muon veto, it is given by the coincidence of a certain number of PMTs, independently of their spatial position inside the water tank. A PMT participates in the coincidence if it fulfils the threshold requirements for individual PMTs. The optimization of the different parameters determing the trigger formation is discussed in this work, aiming at an high tagging efficiency for interesting physical events and reasonable overall trigger rate for the muon veto. As shown below, the best number and geometrical arrangement of the PMTs have been extensively studied with Monte Carlo simulations, as well as the choice to use a reflective foil to cover the internal surface of the water tank; moreover the different possibilities for the trigger condition have been evaluated with this study. In particular the reflective foil selected is DF2000MA by 3M, which provides a very good reflectivity (more than 99% between $\sim$400 and $\sim$1000 nm, as declared by the manufacturer [16] and consistent with what obtained with dedicated experimental measurements, as shown in figure 4), and allows for a shift in the wavelength of the UV Cherenkov photons toward the blue region in order to have a better match with the PMTs' window and photocathode, as stated in a similar study carried out in the framework of the GERDA experiment, using the same reflective foil by 3M (at the time called "VM2000") [18].
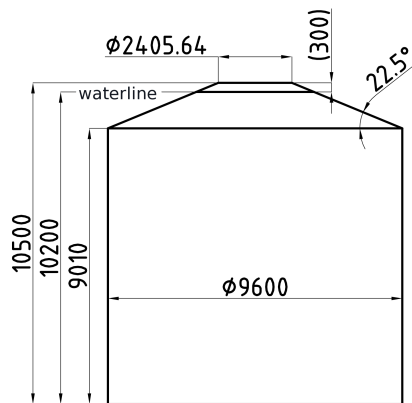

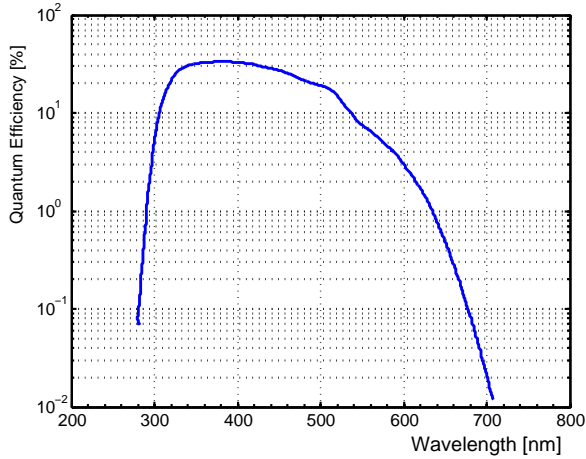Figure 2: Sketch of XENON1T water tank as used in this study.

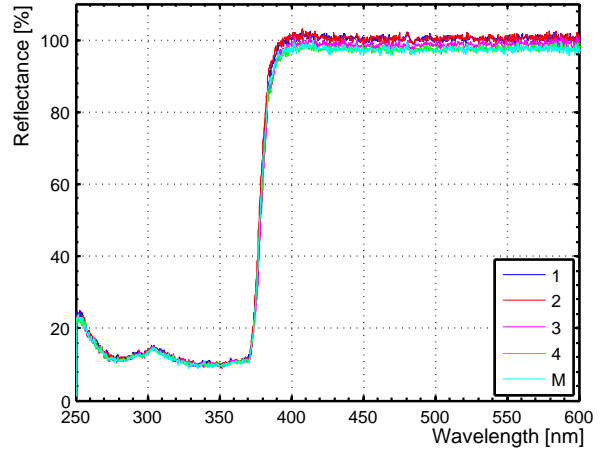Figure 3: Quantum efficiency of one of the HQE Hamamatsu PMTs R5912ASSY [15].

Figure 4: Specular reflectivity measurements of DF2000MA in different positions on the surface of a square shaped foil sample (Edges: 1-4, Middle: M) [17].

3. Description of the Monte Carlo simulation

3.1 Physics inputs

The optimization of the muon veto design has been obtained with a study done through the realization of a detailed Monte Carlo simulation based on GEANT4 [19] version 4.9.3.

The Physics List used considered the following processes:

- muon-induced spallation (or muon photo-nuclear interaction) modeled above 1 GeV muon energy; the final-state generator relies on parametrized hadronic models;

- gamma inelastic scattering (the photo-nuclear interaction) generating its hadronic final states through a chiral-invariant phase-space decay model below 3 GeV; a theoretical quark-gluon string model simulates the punch-through reaction at higher energies;

- hadronic interactions of nucleons, pions and kaons simulated with the quark-gluon string model above 6 GeV, an intra-nuclear binary cascade model at lower energies and a pre-equilibrium de-exitation stage below 70 MeV;

- the equilibrium stage considering fragment and gamma evaporation, fission, Fermi break-up and multi-fragmentation of highly-excited nuclei;

- neutron transport and interaction described by data-driven models below 20 MeV: High-Precision (HP) model;

- elastic scattering of hadrons above 20 MeV described by the *G4LElastic* model;

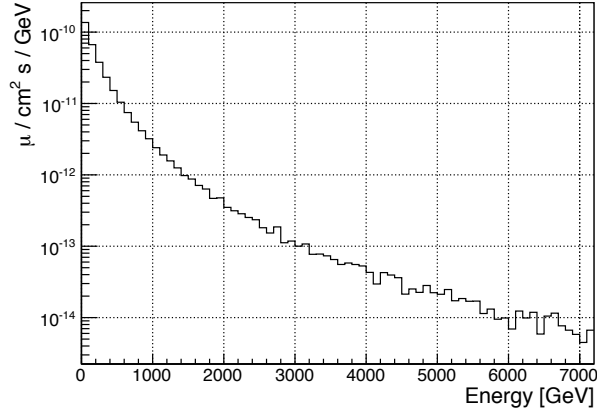- standard treatment of the electromagnetic processes.

Figure 5: Muon energy distribution at LNGS underground laboratory, obtained through the data in [20].

As a first step 10^8 muons were generated with the proper energy and angular distribution (see figures 5 and 6). They were sampled over a large area: a circle with 30 m radius, corresponding to about 3.5 years at LNGS. For the second step 10^4 primary events, each of them containing at least one muon-induced neutron hitting the water tank, were injected in input into a simulation containing a detailed description of the XENON1T geometry.

To study the performances of the muon veto Cherenkov detector the Monte Carlo simulation and the analysis were implemented for two different physical scenarios:

  i) the parent muon passes *inside* the water tank, we will call this "*muon event*";

  ii) the parent muon passes *outside* the water tank, we will call this "*shower event*".

The result of the first step of the Monte Carlo study show that the events of muon-induced neutrons inside the water tank accompanied by the parent muon are ∼ 1/3 of all the cases; for the other 2/3 the muon passes outside. The second case is much more challenging, because here
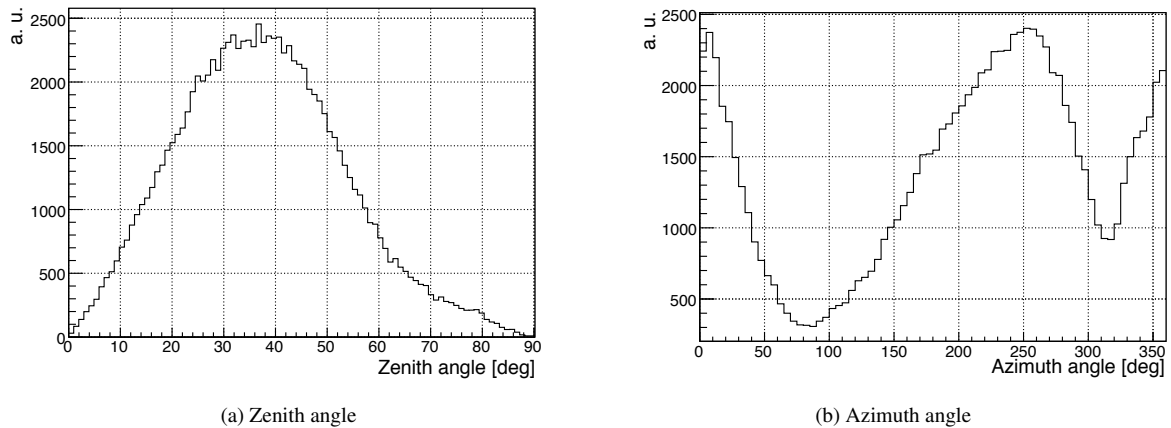

(a) Zenith angle

(b) Azimuth angle

Figure 6: Muon angular distributions at LNGS underground laboratory [20].

we aim to tag the muon-induced neutron just with the Cherenkov light produced by the secondary shower particles hitting the water tank, which is extremely fainter compared to what is produced by a muon.

3.2 Muon veto configurations

As we saw in paragraph 2 the muon veto design is based on the use of several components and each of them can be used in a certain number of different configurations. We have the reflective foil, for which we can vary the type of reflection and the reflectivity percentage, we have the PMTs, for which we can vary the total number employed and the geometrical arrangement and we have the trigger that can work with a different combination of photoelectrons (PE) per PMT and PMT per event. For the optimization of the muon veto efficiency, within the budget constraints, we studied, with Monte Carlo simulations, different set-ups, obtained varying the configuration of each component. The different configurations tested are the following:

- REFLECTOR TYPE:

    - specular;

    - diffusive.

- REFLECTIVITY VALUES:

    - 100% (in all internal surfaces);

    - 95% (lateral and bottom surface);

    - 90% (top surface);

    - 0% (top surface, in all internal surfaces).

- ARRANGEMENT AND TOTAL NUMBER OF PMTS (see figure 7):

    - Position: hexagonal and circular grids, homogenous and non homogenous spacing, with and without lateral side PMTs;

    - Orientation: lateral PMTs looking inwards or 45 deg upwards;

    - Total PMTs employed: 48 - 60 - 72 - 84 - 96 - 108 - 168 - 348 - 1848 - 3504 - 9034.

- SIGNAL THRESHOLDS:

    - to trigger a PMT: from 1 to 20 PE;

    - to trigger an event: from 2 to 5 PMTs.
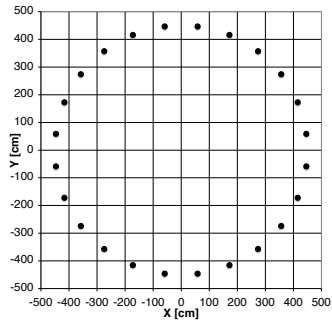
a. Bottom / Top Array Model 1 with 24 PMTs.
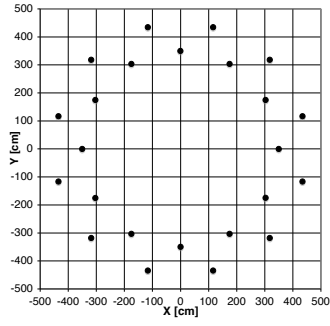
b. Bottom / Top Array Model 2 with 24 PMTs.
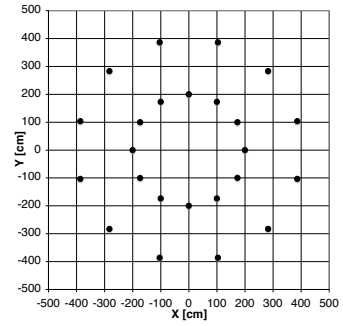
c. Bottom / Top Array Model 3 with 24 PMTs.
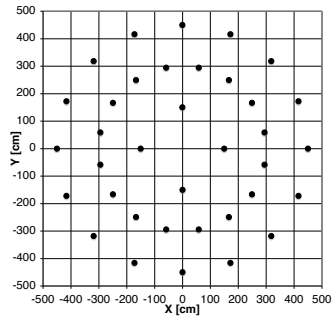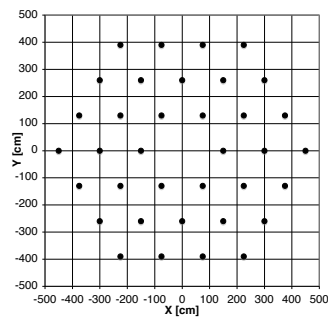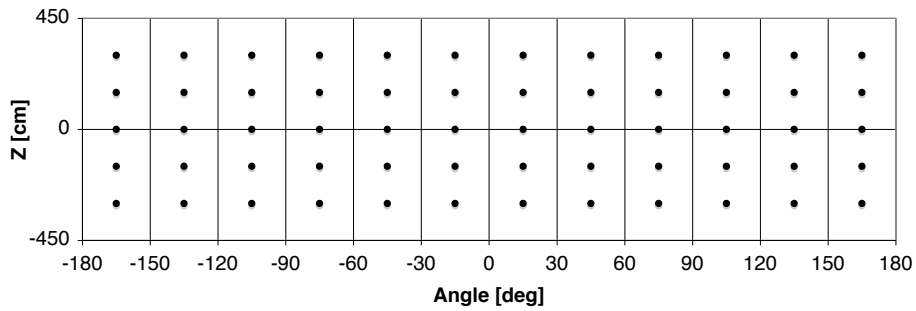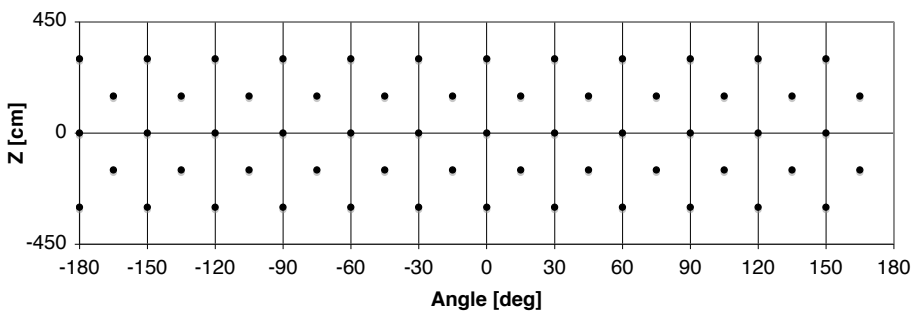
d. Bottom / Top Array Model 4 with 36 PMTs.

e. Bottom / Top Array Model 5 with 36 PMTs.

f. Lateral Array Model 1.

g. Lateral Array Model 2.

Figure 7: All the different PMT arrays tested.

Hit patterns of the Cherenkov photons on the internal surface of the water tank were generated for the different configurations of reflector type and reflectivity levels. Then, with fixed reflector type and reflectivity, we evaluated the efficiency of the muon veto, defined as the percentage of tagged events over all the events hitting the water tank, varying the geometry of the PMTs arrangement. The geometries tested are displayed in figure 7. After that, with the optimized PMTs placement we checked the variation of the efficiency by varying the number of PMTs employed. All those models have been compared with 80 different triggering conditions (from 2 to 5 PMTs in coincidence to trigger an event, and, in each case, from 1 to 20 PE to trigger a PMT). The results obtained are presented in the next paragraph, the errors quoted are the statistical errors.

4. Simulation results

4.1 Reflector type and reflectivity values

The study of the hit pattern of the photons on the internal surface of the water tank shows that, for all the reflectivity values tested, the diffusive reflector possesses a systematically lower percentage of photon survival and a lower efficiency of the vetoing power compared to the specular one; this led to the choice of the specular reflector DF2000MA.

Some of the simulations results are presented in tables 1a and 1b in terms of illumination density (in photons / muon / m^2) and consequent veto efficiency [1] for different reflective foil models.

MUON EVENT			
Model	Illumination density [photons / muon / m^2]		Efficiency [%]
	Bottom	Lateral	
1	2640 ± 40	1640 ± 20	$99.80 \pm 0.05\%$
2	2470 ± 30	1460 ± 20	$99.78 \pm 0.05\%$
3	2380 ± 30	1390 ± 20	$99.75 \pm 0.05\%$
4	2330 ± 30	1330 ± 20	$99.71 \pm 0.06\%$
5	1400 ± 20	655 ± 9	$96.3 \pm 0.2\%$
6	2340 ± 40	1540 ± 30	$99.61 \pm 0.07\%$

(a)

SHOWER EVENT			
Model	Illumination density [photons / muon / m^2]		Efficiency [%]
	Bottom	Lateral	
1	196 ± 12	203 ± 12	$73.3 \pm 0.5\%$
2	182 ± 11	169 ± 10	$71.4 \pm 0.5\%$
3	162 ± 10	162 ± 10	$67.8 \pm 0.5\%$
4	158 ± 10	143 ± 9	$65.9 \pm 0.5\%$
5	96 ± 8	67 ± 4	$42.0 \pm 0.5\%$
6	177 ± 11	144 ± 8	$67.2 \pm 0.5\%$

(b)

Table 1: Bottom and lateral illuminations and efficiency[1] for the muon event (a) and the shower event (b), in the following reflective foil models:
1: Specular reflector. Reflectivity: 100% top - 100% bottom and lateral
2: Specular reflector. Reflectivity: 90% top - 95% bottom and lateral
3: Specular reflector. Reflectivity: 0% top - 100% bottom and lateral
4: Specular reflector. Reflectivity: 0% top - 95% bottom and lateral
5: No reflector
6: Diffusive reflector. Reflectivity: 90% top - 95% bottom and lateral
The selected model is highlighted in grey.

---

[1]The efficiency values have been calculated assuming 84 PMTs arranged with the optimized geometry that will be illustrated in paragraph 4.2

A significant decrease of photons can be revealed while removing completely the reflective foil (compare model 1. with model 5. on tables 1a and 1b); this causes a drastic drop in the efficiency of the veto for the shower event case. Less "dramatic" but still relevant efficiency loss ($\sim 5\%$ again in the shower event case) can be revealed while removing the reflective foil from the top surface (compare model 1. with model 3 on table 1b.). For this reason we decided to clad all (top, lateral and bottom) the internal surfaces of the water tank with the reflective foil.

For what concerns the final calculation of the efficiency of our detector, the reflectivity values that will be taken into account are those obtained with the experimental measurements reported in [17] and shown in the curve in figure 4. Anyway, in order to take into account, with a conservative approach, the difficulties in attaching the foil perfectly, especially on the top surface of the tank, the values in the plateau of the curve between 400 nm and 600 nm, will be replaced with the values of the foil model 2.

In figure 8 we show the light distributions (illumination density averaged over 10^4 primary events) on the tank's internal surfaces, bottom on letters (a) and (c) and lateral on letters (b) and (d), in the case of a specular reflector with the above mentioned choice for the reflectivity values for the muon event case and the shower event case, respectively.
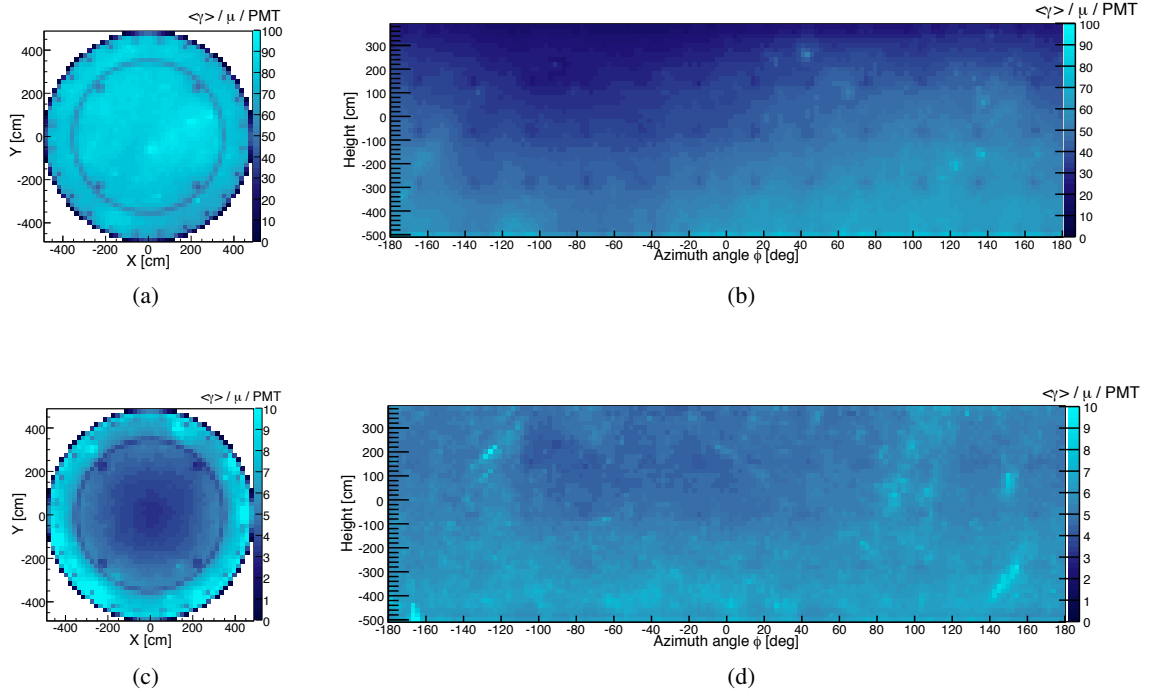
Figure 8: Bottom (on the left) and lateral (on the right) illuminations for muon events, (a) and (b), in the selected model (n.2 in table 1a) and the shower events, (c) and (d), in the selected model (n.2 in table 1b). Illumination values averaged over 10^4 primary events. From those pictures, we can identify the shadow of the objects very close to the surfaces, such as pipes, the support structure for the dark matter detector, and the muon veto PMTs arranged as in the optimized geometry illustrated in paragraph 4.2.

4.2 Arrangement and total number of PMTs

The comparison of all the different PMT geometries tested (results can be seen in table 2 for the shower event case) led to the conclusion that the best way to arrange PMTs, both for the muon event case and for the shower event case, is:

- TOP ARRAY: a ring at vertical height of 9 m from ground floor (the top edge of the cylindrical part of the tank), at radius 4.5 m, with the PMTs looking downward;

- LATERAL ARRAY: rings equally spaced vertically, attached to the tank's surface, with the PMTs looking inward;

- BOTTOM ARRAY: a ring in the bottom surface of the tank, at radius 4.5 m, with the PMTs looking upward.

In fact as we can see from the results obtained, the bottom and top grids give the best contribution to the efficiency when the PMTs are arranged very close to the external border of the circular area, rather than when they are spread all over the area itself. The reasons are explained below:

- for the muons: the muons traveling >1 m in water are surely tagged thanks to the enormous amount of light they produce, and the only events that could escape tagging are the so called "border events" constituted by those muons that cross the water tank just in the outermost layer of water. Placing the PMTs in those border areas enhances the possibility to recover a fraction of those events.

- for the showers: most of the light from the shower events is deposited in the very external part of the water volume, so it is there where we have the highest chance to capture these more elusive events.

Table 2: Efficiency in tagging shower events with different arrays of PMTs. The efficiency values have been calculated assuming the triggering requirements as it will be illustrated in paragraph 4.3.

SHOWER EVENT			
Array	Model	Nb	Efficiency [%] (shower event)
TOP	1	24	45.1 ± 0.5
TOP	2	24	42.6 ± 0.5
TOP	3	24	37.2 ± 0.5
TOP	4	36	49.9 ± 0.5
TOP	5	36	49.3 ± 0.5
LATERAL	1	24	43.4 ± 0.5
LATERAL	2	24	43.3 ± 0.5
LATERAL	1	36	53.0 ± 0.5
LATERAL	2	36	52.9 ± 0.5
BOTTOM	1	24	44.4 ± 0.5
BOTTOM	2	24	42.3 ± 0.5
BOTTOM	3	24	39.1 ± 0.5
BOTTOM	4	36	50.5 ± 0.5
BOTTOM	5	36	49.2 ± 0.5

For the lateral grids the results obtained proved that no difference exists in placing them vertically aligned (like in figure 7f) or staggered (like in figure 7g). For mechanical reasons, it is easier to construct rails for the PMT holders in the first configuration of these two, so this was the one adopted. Moreover, no improvement was obtained using a 45-deg inclination upward compared to the case with the PMTs looking inward.

With the above mentioned optimized arrays, different total number of PMTs have been tried in order to obtained satisfactory values of efficiency. In particular, high performances, $(99.61\pm0.07)\%$, in tagging "muon events" can be achieved with just 48 PMTs: 24 in the bottom array and 24 in the top array. Studying the "shower event" tagging, we find that, in order to obtain high performances, we need to increase the total number of PMTs by adding rings of PMTs to the lateral surface of the tank.

In table 3, we present the results of the efficiency in tagging "shower events" using 24 PMTs on bottom and 24 PMTs on top, with the optimized arrangement just mentioned, versus an increasing number of lateral PMTs from 0 to 3456. Each time one or more rings of 12 PMTs was added, with a consequent increase in the total number of PMTs from 48 to 3504. In the last entry of table 3, we have the configuration with the water tank surfaces completely covered with PMTs, including the bottom and top array (for the top array in this case we use all the conical surface to place PMTs). With this last configuration, we can estimate the fraction of 'untaggable' events, that is, the fraction of events that, by their nature, produce so little light as to be invisible with whatever level of detector optimization. As we see from the table $\sim$10% of the shower events are untaggable. Instead, to obtain at least 70% efficiency in tagging showers, we need to employ 84 PMTs (24 in one ring in the top array, 36 in three rings of 12 PMTs each in the lateral array, 24 in one ring in the bottom array). This is the final configuration we decided to employ, as it is a reasonable compromise between performance and cost.

SHOWER EVENT				
Total PMTs	Top array	Lateral array	Bottom array	Efficiency [%]
48	24	0	24	61.3 ± 0.5
60	24	12	24	65.6 ± 0.5
72	24	24	24	68.7 ± 0.5
84	24	36	24	71.4 ± 0.5
96	24	48	24	72.6 ± 0.5
108	24	60	24	74.7 ± 0.5
168	24	120	24	79.5 ± 0.4
348	24	300	24	85.3 ± 0.4
1848	24	1800	24	89.0 ± 0.3
3504	24	3456	24	89.9 ± 0.3
9034	1589	5699	1746	90.9 ± 0.3

Table 3: Efficiency in tagging shower events for different total number of PMTs (in grey box the selected case). The last values reference the configuration with a complete coverage of the WT with PMTs. The efficiency values have been calculated assuming the triggering requirements as it will be illustrated in paragraph 4.3.
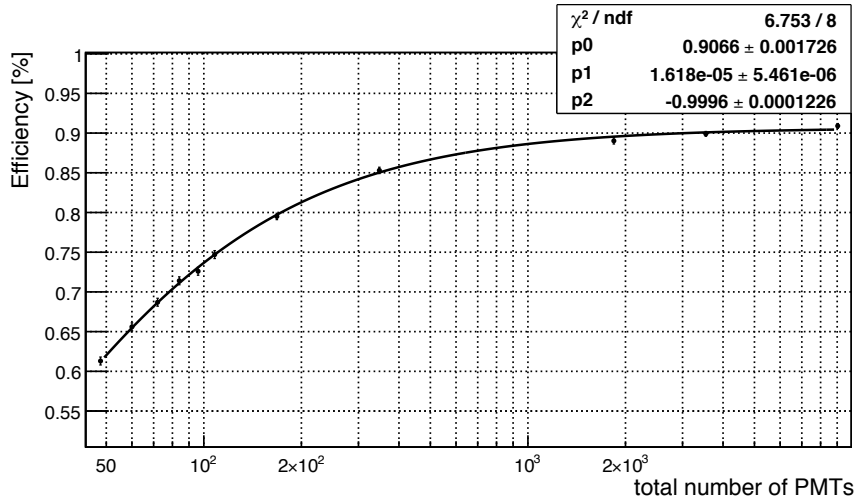
Figure 9: Efficiency in tagging shower events vs. an increasing number of PMTs employed in the previously optimized array geometry. The efficiency values have been calculated assuming the triggering requirements as it will be illustrated in paragraph 4.3.

The values in table 3 are plotted in the graph shown in figure 9 and fitted with a sigmoid function:

$$f(x) = p0 \cdot \frac{1 - e^{-x \cdot p1}}{1 + p2 \cdot e^{-x \cdot p1}}$$

where the parameters:

- p0 = 0.9066 ± 0.0017

- p1 = (1.6 ± 0.5) · 10^{-5}

- p2 = -0.99963 ± 0.00012

are correlated to:

- p0: the limit of taggable events: ∼90%

- p1 and p2:

    - the ratio between the sensitive area (photocathode) and the hittable area (water tank surface): ∼ $1.9 \cdot 10^{-5}$;

    - the impact of the reflective foil;

    - the impact of the trigger request: 4 PMTs in coincidence within 300 ns (as we will see in paragraph 4.3).

4.3 Trigger condition

The signal from each PMT of the muon veto will be digitized at 100 MSamples/s. Two free parameters determine the condition for which a single PMT participates in the trigger formation:

- threshold (*thr*), the minimum amplitude that a single sample has to exceed. It can be expressed as a fraction of the mean amplitude of a single PE;

- time over threshold (*tot*), the number of consecutive samples above threshold.

A single PMT partecipates in forming the trigger if its signal has an amplitude greater than *thr* for at least *tot* consecutive samples. The trigger condition for the muon veto will be the coincidence of ≥N PMTs inside a time window Δt, independently on their position inside the water tank. The optimal width for Δt, has been determined looking at the distributions of the time difference of photons arriving on PMTs photocatodes in the simulation of muon events and shower events, an example is shown in figure 10 for the 4-fold coincidence. In the following the time window is fixed to Δt = 300 ns.

### 4.3.1 Tagging efficiency depending on trigger requirements

The efficiency for tagging muon events and shower events depending on trigger requirements has been obtained from Monte Carlo, with 84 PMTs arranged in the best configuration and with full efficiency in detecting PE. Figure 11 shows the results depending on the number of PE detected by individual PMTs and for different number N of PMTs in coincidence. It appears that, in order to keep a reasonable tagging efficiency for the shower events (>60%), it is necessary to work at the single PE detection level. The choice of the number N of PMTs in coincidence will be done with the goal to get the highest tagging efficiency while having a suitable trigger rate, as discussed in 4.3.2. Muon events are much less affected by the trigger conditions as their tagging efficiency is close to 100% in many different cases.

4.3.2 Expected trigger rate for the muon veto

We studied the behaviour of the PMT dark counting rate R_d(*thr*, *tot*) with *thr* varying in the interval 0.25-1.0 PE for *tot*=1 and *tot*=2. For each of these cases we determined the efficiency η(*thr*, *tot*) for detecting a single PE, which is reported in figure 12. To get an estimation of the counting rate of a single PMT in the muon veto, R_s(*thr*, *tot*), we have to consider the contribution of the Cherenkov light induced by secondary electrons as a product of the interaction of gammas and neutrons from natural radioactivity in water. The flux of radioactive decay particles from rock and concrete in LNGS halls is assumed 1 γ / cm^2 / s [22], [23] and $5 \cdot 10^{-6}$ neutrons / cm^2 / s [23], [24]. For the radioactive contaminations of the stainless steel we use the results in [25], multiplied by a factor 100 in order to get a very conservative approach, given that the stainless steel of XENON100, discussed in that paper, is highly radio-pure. A dedicated Monte Carlo shows that the only important contribution comes from γ emitted in the rock, which on average induce on each PMT a rate of Rb~2000 PE/s. We expect that the largest contribution to the trigger rate as long as N≤5 is due to the accidental coincidences inside Δt. These can be calculated as follows:
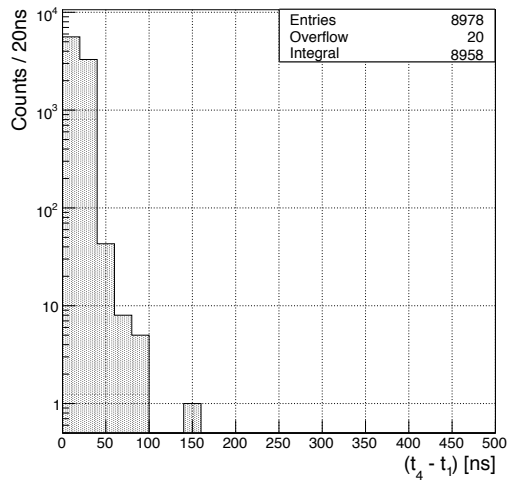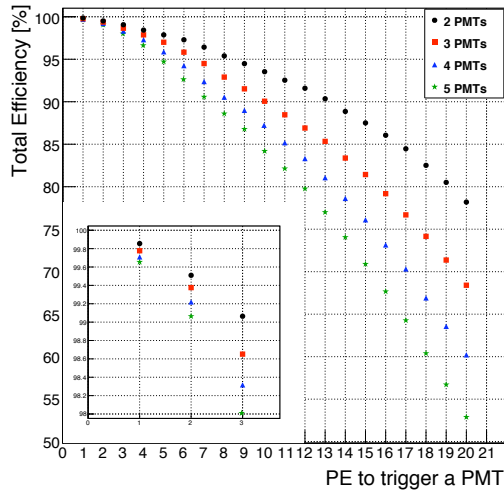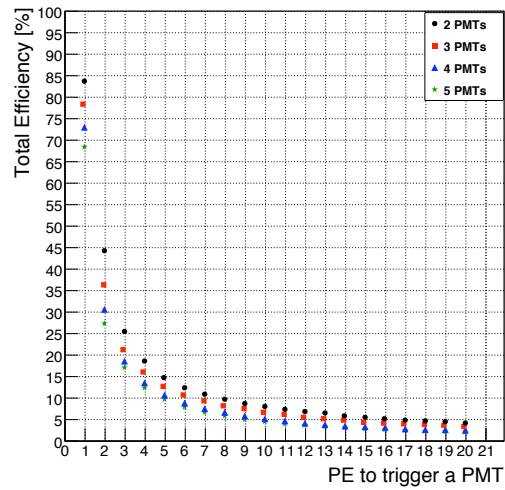
(a) Mu-event case
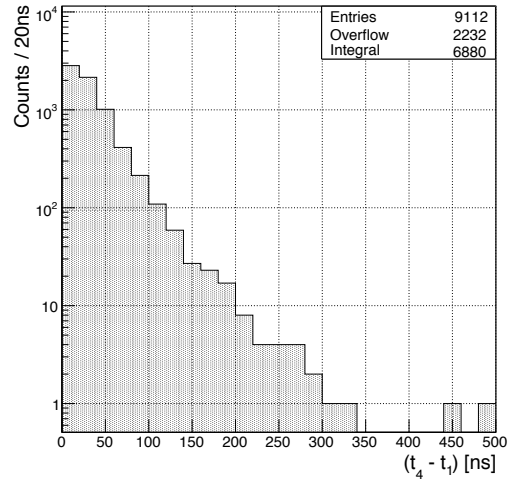
(b) Shower-event case

Figure 10: Distribution of maximum time difference of photons arriving on the PMTs photocathodes in a 4-fold coincidence with the selected model (n. 2 of table 1) for the reflective foil and 84 PMTs in the optimized geometry. In the inset:

- Entries: primary events hitting the water tank (out of 10^4 generated)
- Overflow: events with less than 4 PMTs on or with 4 PMTs on within more than 500 ns
- Integral: events with at least 4 PMTs on within 500ns. In the muon event case this value is coincident with the tagged events, since all the time differences, between 0 and 500 ns, are < 300 ns

(a) Mu-event case

(b) Shower-event case

Figure 11: Curves of the efficiency versus the triggering requirements with the selected model (n. 2 of table 1) for the reflective foil and 84 PMTs arranged with the optimized geometry.

$$R_{\geq N} = \sum_{j=N}^{M} R_{j-1} \cdot (M - j + 1) \cdot R_s(thr,tot) \cdot \frac{\Delta t}{(j-1)}$$

- $R_s(thr,tot)$ is the single PMT counting rate calculated as: $R_s(thr,tot) = R_d + \eta \cdot R_b$

- $R_1 = M \cdot R_s$

- M=84 is the total number of PMTs.

We also expect to observe scintillation of α particles in the DF2000MA reflective foil. There are hints for the observation of this effect in GERDA water tank [21], where the same kind of reflective foil is installed. We derived an upper limit on the expected scintillation rate of α thanks to dedicated measurements of the scintillating properties of the foil. The contribution to the muon veto trigger rate remains subdominant with respect to accidental coincidences for a number of PMTs in coincidence N≤5.

Finally we have the trigger rate induced by muons passing through the water tank (with or without accompanying neutron) and shower events. Considering the dimensions of the water tank we may expect a rate $R_\mu \sim 5 \cdot 10^{-2}$ s^{-1} of muons passing through the water tank and an even lower rate due to shower events

Figure 13 reports the muon veto trigger rate depending on thr with the coincidence of $\geq$ N PMTs inside Δt, for N=3 (continuous lines), N=4 (short dashed lines) and N=5 (dotted dashed lines) and for tot=1 (thick lines) and tot=2 (thin lines). With N=3 the expected trigger rate is higher than 100 s^{-1} at least when the efficiency for detecting PE is better than 50%. With N=4 a good efficiency $\eta > 90\%$ can be achieved both with tot=1 and tot=2 while keeping the trigger rate lower than 20 s^{-1}. In the case N=5 the trigger rate can be lower than 1 s^{-1} having high efficiency in detecting PE.
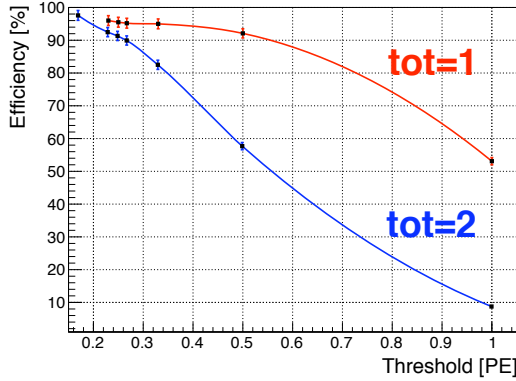

Figure 12: The efficiency η in detecting PE depending on *thr* for *tot* = 1 and *tot* = 2.
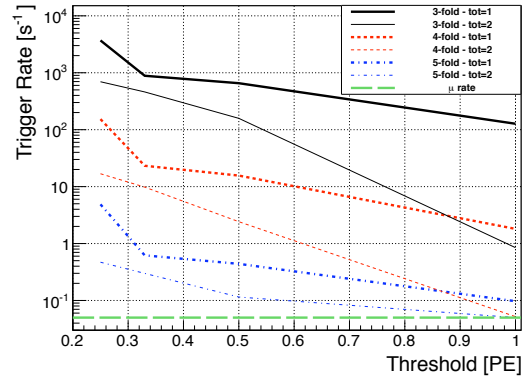
Figure 13: Muon veto trigger rate depending on *thr* for N = 3 (continuous lines), N = 4 (short dashed lines) and N = 5 (dotted dashed lines) and for tot = 1 (thick lines) and *tot* = 2 (thin lines). The horizontal long dashed line marks the contribution from muon and shower events.

4.4 Summary of the final configuration

In conclusion using:

- Specular reflector (DF2000MA) with reflectivity curve as measured in [17] and shown in figure 4, with the plateau of the curve between 400 and 600 nm modified according to model 2 of table 1;

- 84 PMTs (HQE 8" Hamamatsu R5912ASSY) with quantum efficiency, averaged over the Cherenkov light wavelength distribution, of about 30 % (figure 3), and arranged as in the conclusion of section 4.2 (see also figure 14);

- trigger at single PE (trigger efficiency 100%) in a 4-fold coincidence of 300 ns time window.

the efficiency of the XENON1T water Cherenkov detector to veto muon-induced neutrons hitting the water tank is:

- $(99.78 \pm 0.05)\%$ for the "muon event" case ($\sim$1/3 of the total events);

- $(72.2 \pm 0.5)\%$ for the "shower event" case ($\sim$2/3 of the total events).

where the "total events" are all those in which the muon generated produces at least one neutron hitting the water tank.
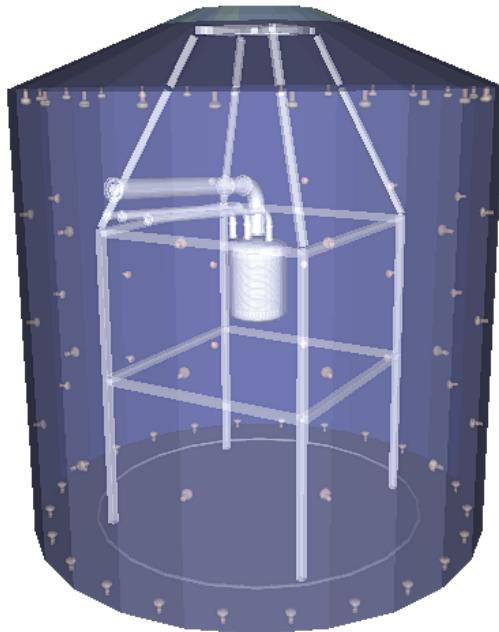

Figure 14: 3D-Graphical output of the Monte Carlo geometry.

4.5 XENON1T update: XENONnT

After the main part of the study presented here has been finalized, the collaboration decided to dimension most sub-systems of the XENON1T experiment such that it can easily be upgraded to an instrument featuring more than 7 tonnes of LXe. In particular all LXe handling systems, the detector support structure, as well as the outer cryostat are now already larger than required for the initial phase. We have verified that the results presented here are unaffected by these changes. For what concerns the muon veto, the operation is the same both for the XENON1T detector as well as for the upgraded detector.

5. Conclusions

For the future XENON1T detector, the goal of sensitivity of $2 \cdot 10^{-47}$ cm^2 implies a background reduction of two orders of magnitude compared to the level of the current XENON100 detector. This background reduction requirement, together with its location at the LNGS laboratory, necessitates the construction of a muon veto.

The type of muon veto chosen is a water Cherenkov detector based on a water tank equipped with PMTs and a reflector foil. In this work, we have studied the optimization of its efficiency in tagging muon-induced neutrons through the Cherenkov light produced in water by the parent muon and/or the other muon-induced secondary particles. Specifically, we determined the most cost effective of reflector type (studying also different reflectivity levels), PMT number and arrangement, and signal thresholds, to optimize the above mentioned efficiency, in both cases where we have or do not have the muon accompanying the neutron in the tank. The analysis of all the generated data proved, in particular, that the most convenient choice for the reflector is a specular one and, for the PMTs, a good choice is a total of 84 arranged in 5 grids (1 top, 3 lateral and 1 bottom).

Moreover, considering the outcomes of a dedicated study on the trigger implementation, we found that it is possible to work at the single PE detection level on the single PMT requiring a 4-fold or 5-fold coincidence in a 300 ns time window.

The efficiency obtained in tagging muons that enter the water tank, with the Cherenkov detector constructed as described, is $> 99.5\%$; these events represent $\sim 1/3$ of the cases where we have the muon-induced neutron inside the water tank. For the other $\sim 2/3$ of the cases, thanks to the Cherenkov light produced in the water by secondary particles of the muon-induced shower, we are able to reach a tagging efficiency of $> 70\%$. None of those results take into account the wavelength shifting power of the reflector foil and are based on reflectivity values lower than that declared by the manufacturer of DF2000MA foil.

Conclusions remain valid for the upgrade of the experiment, XENONnT, with a target mass up to more than 7 tonnes.

Acknowledgments

References

[1] Jonathan L. Feng, *Dark matter candidates from particle physics and methods of detection*, *Annual Review of Astronomy and Astrophysics* Vol. **48**: 495-545, (2010) [astro-ph.CO/1003.0904].

[2] J. Angle et al., *First results from the XENON10 dark matter experiment at the Gran Sasso national laboratory*, *Phys. Rev. Lett.* **100**, (2008) 021303 [astro-ph/0706.0039].

[3] J. Angle et al., *Limits on spin-dependent WIMP-nucleon cross sections from the XENON10 experiment*, *Phys. Rev. Lett.* **101**, (2008) 091301 [astro-ph/0805.2939].

[4] E. Aprile et al., *Dark matter results from 225 live days of XENON100 data*, *Phys. Rev. Lett.* **109**, (2012) 181301 [astro-ph.CO/1207.5988].

[5] E. Aprile et al., *Limits on spin-dependent WIMP-nucleon cross sections from 225 live days of XENON100 data*, *Phys. Rev. Lett.* **111**, (2013) 021301 [astro-ph.CO/1301.6620].

[6] E. Aprile, XENON1T collaboration, *The XENON1T dark matter search experiment*, *Proceedings of DM2012 at UCLA* astro-ph.IM/1206.6288.

[7] E. Aprile et al., *Study of the electromagnetic background in the XENON100 experiment*, *Phys. Rev. D* **83**, (2011) 082001 [astro-ph.IM/1101.3866].

[8] E. Aprile et al., *The neutron background of the XENON100 dark matter experiment*, *J.~Phys.~G:~Nucl.~Part.~Phys.* **40**, (2013)115201 astro-ph.IM/1306.2303.

[9] M. Aglietta et al., *Muon depth-intensity relation measured by LVD underground experiment and cosmic-ray muon spectrum at sea level*, *Phys. Rev. D* **58**, (1998) 92005 [hep-ex/9806001].

[10] V. A. Kudryavtsev, L. Pandola and V. Tomasello, *Neutron- and muon- induced background in underground physics experiments*, *Eur.~Phys.~J.~A* **36**, (2008) 171-180. [0802.3566 [astro-ph]].

[11] M. Selvi (for the LVD coll.), *Analysis of the seasonal modulation of the cosmic muon flux in the LVD detector during 2001-2008*, *Proceedings of the* **31st**, ICRC (2009)

[12] M. Ambrosio et al., *Measurement of the residual energy of muons in the Gran Sasso underground Laboratories*, *Astropart.Phys.* **19**, (2003), 313-328 [hep-ex/0207043].

[13] A. Ferrari, P.R. Sala, A. Fasso, and J. Ranft, *FLUKA: a multi-particle transport code*, *CERN-2005-10 INFN/TC-05/11 SLAC-R-773* (2005).

[14] D.-M. Mei, A. Hime, *Muon-induced background study for underground laboratories*, *Phys. Rev.D* **73**, (2006) 053004 [hep-ph/0512125].

[15] *Hamamatsu Photonics K.K.*, *Hamamatsu Official Site*.

[16] *3M Company*, *3M Official Site*.

[17] C. W. Geis, *Untersuchung der DF2000MA Reflektorfolie in Hinsicht auf ihre Verwendung im XENON1T MuonVeto*, *Research thesis, Johannes Gutenberg University Mainz, (2012)*.

[18] M. Knapp et al., *The GERDA muon veto Cherenkov detector*, *Nucl. Instr. Meth. A* **610**, (2009).

[19] S. Agostinelli et al., *Geant4-a simulation toolkit*, *Nucl. Instr. Meth. A* **506**, (2003).

[20] M. Aglietta et al., *Single muon angular distributions observed in the LVD particle astrophysics experiment*, *Astropart.Phys.* **2**, (1994).

[21] K.-H. Ackermann et al., *The GERDA experiment for the search of $0\nu\beta\beta$ decay in ^{76}Ge*, *Eur.Phys.J. C* **73:2330** (2013)

[22] C. Arpesella et al., *Background measurements at Gran Sasso Laboratory*, *Nucl. Physics. B (Proc.Suppl)* **28A**, (1992).

[23] S. Fattori, *Study of Radioactive Background Minimization for a 1 Ton Module of the XENON Experiment INFN PhD Thesis* (8 lug 2010).

[24] P. Belli et al., *Deep underground neutron flux measurement with large BF_3 counters*, *Il Nuovo Cimento A* **101-6**, (1989)

[25] E. Aprile et al., *Material screening and selection for XENON100*, *Astropart.Phys.* **35-2**, (2011) 015 [physics.ins-det/1103.5831v2].